# Structural and magnetic properties of $La_{0.7}Sr_{0.1}Ag_xMnO_{3-\delta}$ perovskite manganites*

Hou Xue(侯 雪)[a], Ji Deng-Hui(纪登辉)[a)b)], Qi Wei-Hua(齐伟华)[a)†],
Tang Gui-De(唐贵德)[a], and Li Zhuang-Zhi(李壮志)[a)]

[a)] *Hebei Advanced Thin Film Laboratory, Department of Physics, Hebei Normal University, Shijiazhuang* 050024, *China*
[b)] *Department of Physics and Electronic Science, Liupanshui Normal University, Liupanshui* 553004, *China*

(Received 10 October 2014; revised manuscript received 15 December 2014; published online 27 March 2015)

Ag-doped manganite powder samples, $La_{0.7}Sr_{0.1}Ag_xMnO_{3-\delta}$ ($x = 0.00$, 0.025, 0.05, 0.075, and 0.10) were synthesized using the sol–gel method. X-ray diffraction patterns indicated that the samples had two phases with the $R\bar{3}c$ perovskite being the dominant phase and $Mn_3O_4$ being the second phase. X-ray energy dispersive spectra indicated that the ratio of Ag to La was very close to that of the nominal composition in the samples. The specific saturation magnetizations at 300 K increased from 32.0 A·m$^2$/kg when $x = 0.00$ to 46.8 A·m$^2$/kg when $x = 0.10$. The Curie temperature, $T_C$, of the samples increased from 310 K when $x = 0.00$ to 328 K when $x = 0.10$. Because the atomic concentration ratios of La, Sr, and Mn in the five samples were all the same and only the Ag concentration changed, the variations of the specific saturation magnetizations at 300 K and the Curie temperatures suggested that the Ag cations have been doped into the *A* sites of the perovskite phase in the samples.

**Keywords:** perovskite manganite, Curie temperature, cation vacancy, crystal structure

**PACS:** 75.47.Lx, 75.50.Dd, 74.25.Ha, 91.60.Ed **DOI:** 10.1088/1674-1056/24/5/057501

## 1. Introduction

As electronic systems with strong correlations, perovskite manganese oxides with an $ABO_3$ structure have rich physical and chemical properties,[1–8] and have been the subject of extensive attention, both experimentally and theoretically. Starting with the manganese oxide $LaMnO_3$, bivalent alkaline earth metal or univalent alkali metal ions can substitute for the trivalent La ions. Typical examples have the general formula $La_{1-x}M_xMnO_3$ ($M$ = Ca, Ba, Sr, Pb, etc). The valence state and ionic radius of the doping ions at the *A*-sites affect the valence of the Mn ions at the *B* sites, and cause lattice distortion.

These compounds exhibit a number of interesting physical phenomena, including ferromagnetism, colossal magnetoresistance, and spin glass states. It has also been found that the Curie temperatures and the content of $Mn^{4+}$ cations in $La_{0.7-x}Sr_xMnO_3$ ($0.1 \leq x \leq 0.3$) samples increase with increasing $x$.[1] In order to explain these phenomena, Zener[9] proposed the double exchange mechanism controlled by the displacement of $e_g$ electrons from $Mn^{3+}$ to $Mn^{4+}$ sites mediated by an $O^{2-}$ ion.

For the self-doped manganites, such as $La_{1-x}MnO_3$, a number of researchers have assumed that there were vacancies at the *A* sites and that the number of vacancies was related to the self-doping level.[10–15] However, the available volume of the *B* sites was smaller than that of the *A* sites in the $ABO_3$ perovskite structure. Therefore, based on the thermal equilibrium theory of crystal defects, our group[16] proposed that, in fact, there should be no cation vacancies at the *A* sites related to the self-doping level. A part of $Mn^{2+}$ cations existed in *A* site of this kind of materials,[8,16] which were proved using experimental method.[17,18] Abou-Ras *et al.*[17] prepared self-doped perovskite manganite powder samples of composition $Pr_{0.7}Sr_{0.3-x}MnO_{3-\delta}$ ($x \leq 0.2$), and found, using the $^{55}Mn$ nuclear magnetic resonance technique, that the $Mn^{2+}$ content increased as the self-doping level $x$ increasing. Ulyanov *et al.*[18] prepared Ti-doped, *A*-site deficient $La_{0.6}Sr_{0.4-x}Ti_xMnO_{3-\delta}$ ($x \leq 0.15$) manganites, and using x-ray absorption finite structure studies, found that the Ti ions entered the *B* sites, instead of the *A* sites, while there were $Mn^{2+}$ ions at the *A* sites.

There have been several reports in the literature concerning Ag-doping perovskite manganites.[19–22] However, there are distinctly different views between these reports concerning whether Ag cations can dope into the perovskite phase. Tao *et al.*[19] synthesized a series of Ag-doped samples of $La_{1-x}Ag_xMnO_3$ by solid-state reaction method. Using x-ray diffraction spectra, they concluded that only the perovskite phase was present in the samples with $x \leq 0.25$, and that there was a nonmagnetic metal Ag phase in addition to the perovskite phase in the samples with $x > 0.25$. However, other researchers[20,21] have considered that Ag ions could not be

*Project supported by the National Natural Science Foundation of China (Grant No. NSF-11174069), the Natural Science Foundation of Hebei Province, China (Grant No. E2011205083), the Key Item Science Foundation of Hebei Province, China (Grant No. 10965125D), the Key Item Science Foundation of the Education Department of Hebei Province, China (Grant No. ZD2010129), and the Young Scholar Science Foundation of the Education Department of Hebei Province, China (Grant No. QN20131008).

†Corresponding author. E-mail: qiweihua1028@126.com

© 2015 Chinese Physical Society and IOP Publishing Ltd 

doped into the *A* sites of the perovskite structure. In particular, Xu *et al.*[22] performed EELS (electron-energy-loss spectroscopy) studies for samples prepared by Tao *et al.* They found that the perovskite phase included only La, Mn, and O in the EELS spectrum. Since Ag particles were observed in SEM photos, they concluded that Ag could not be doped into the perovskite phase.

Our group reported the structures and the magnetic property of self-doped manganites $La_{0.7-x}Sr_{0.3}Mn_1O_3$,[23] $La_{0.8-x}Sr_{0.2}MnO_3$,[24] $La_{0.6-x}Sr_{0.4}MnO_3$,[25] and $La_{0.7}Sr_{0.3-x}MnO_3$.[26] We explained why there were $Mn_3O_4$ second phase in those samples when self-doping level was higher than a certain level.[23] In this work, in order to determine whether silver can dope into the *A* sites of the perovskite structure, we doped Ag in the self-doped manganites $La_{0.7}Sr_{0.1}MnO_3$ contained the $Mn_3O_4$ second phase, prepared samples with the nominal composition $La_{0.7}Sr_{0.1}Ag_xMnO_{3-\delta}$ using the sol–gel method. The crystal structure, the elemental content, the ion distribution, and the magnetic property of the samples have been investigated. All the experimental results indicate that the silver cations have been successfully doped into the *A* sites.

## 2. Experiment

Powder samples with the nominal composition $La_{0.7}Sr_{0.1}Ag_xMnO_{3-\delta}$ ($0.00 \leq x \leq 0.10$) were synthesized using the sol–gel method.[27,28] Stoichiometric amounts of the high purity chemicals $La_2O_3$, $Sr(NO_3)_2$, $AgNO_3$, and $Mn(NO_3)_2$ were dissolved in dilute $HNO_3$ solution with PH = 3. Citric acid and ethylene glycol were then added to the solution as complexing agents for the metal ions. The molar ratios of citric acid to ethylene glycol and to the sample were 5.3:5.3:1.0. This solution was placed in a water bath at 363 K and slowly evaporated until a gel formed. This gel was heated at 473 K for 24 h until completely dry. After grinding, the powders were subjected to further heat treatment. The protocol for increasing the temperature was altered from the usual heat treatment in which the temperature is increased directly from 473 K to 773 K. In our procedure, the temperature was increased in steps of 50 K, from 473 K to 773 K, with 30 min spent at each step. The powders were then thermally treated at 773 K for 6 h, and were gradually cooled during furnace cooling. This improved procedure which results in slow decomposition of the organic precursor, may be a key improvement for doping Ag into the perovskite phase. After grinding, the powder was again thermally treated at 873 K for 5 h. Subsequently, the samples were calcined in air at 1073 K for 10 h and gradually cooled during furnace cooling. According to Ref. [28], the highest calcined temperature $T_{\rm Cal} = 1073$ K is the best heat treatment condition, at which condition the content ratio A:B:O is very close to 1:1:3.

The crystal structures of the samples were identified through x-ray diffraction (XRD) using an X'pert Pro x-ray diffractometer with Cu $K_\alpha$ ($\lambda = 1.5406$ Å) radiation at room temperature. The data were collected in the $2\theta$ range of 20°–120° with a step size of 0.01671°. The composition of the samples was analyzed by x-ray energy-dispersive spectra (EDS) at room temperature, using an INCA PentaFETx3 system, with an accelerating voltage of 20 kV. The magnetic field and temperature dependence of the specific magnetization, $\sigma(H)$ and $\sigma(T)$, of the powder samples were measured using a physical properties measurements system (PPMS, Quantum Design Corporation, USA). We defined the temperature at which the $\mathrm{d}\sigma/\mathrm{d}T$ reached its minimum value as the Curie temperature ($T_{\rm C}$). The Curie temperatures of the samples were measured under an applied magnetic field 0.05 T.

## 3. Results and discussion

### 3.1. Structural analysis

Figure 1(a) shows the x-ray diffraction patterns for the $La_{0.7}Sr_{0.1}Ag_xMnO_{3-\delta}$ samples, which are similar to those of self-doped manganites reported by our group,[23–26] indicate that the samples have two phases with the rhombohedral perovskite, $R\bar{3}c$ space group, being the dominant phase and tetragonal $Mn_3O_4$ being the second phase. From Fig. 1(b), it can be seen that the peak intensities of the $Mn_3O_4$ phase decrease with increasing doping level *x*.

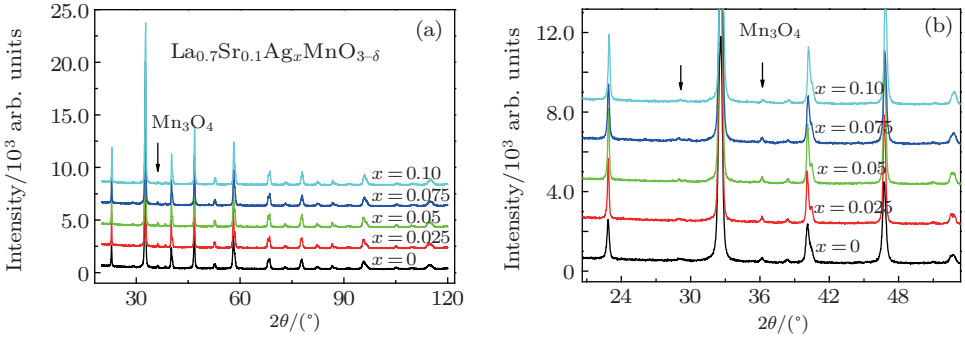



**Fig. 1.** (color online) (a) XRD patterns for the samples with nominal composition $La_{0.7}Sr_{0.1}Ag_xMnO_{3-\delta}$. All the samples exhibit two phases, a perovskite main phase, and a $Mn_3O_4$ second phase for which the main diffraction peaks are marked by the symbol "↓". (b) Enlarged image of panel (a).

Using the X'Pert HighScore Plus software, we calculated the volume averaged crystallite diameters, $D$, of the samples using the Scherrer equation, and found the diameters of 39, 78, 77, 53, and 54 nm, corresponding to $x = 0.00$, 0.025, 0.05, 0.075, and 0.10, respectively.

Table 1 shows the phase analysis data for the $La_{0.7}Sr_{0.1}Ag_xMnO_{3-\delta}$ samples, obtained by fitting the XRD spectra. In this way, we obtained the zeroth-order approximation of the cell volume $V_C$ of the perovskite phase in the samples.

**Table 1.** The XRD main peak areas ($A_P$ and $A_M$) of the perovskite phase and $Mn_3O_4$ phase in the samples with the nominal composition $La_{0.7}Sr_{0.1}Ag_xMnO_{3-\delta}$; the molar content $y$ of Mn in $Mn_3O_4$ phase, calculated from the XRD main peak area ratios $A_M/A_P$; cell volume $V_C$, parameter $c_M$.

| No | $x$ | $A_P$ | $A_M$ | $A_M/A_P$ | $V_C$ | $c_M$ | $y$ |
|---|---|---|---|---|---|---|---|
| $A_1$ | 0.000 | 1657.9 | 56.16 | 0.0339 | 350.8 | 15.02 | 0.1613 |
| $A_2$ | 0.025 | 1614.9 | 50.26 | 0.0311 | 351.0 | 13.80 | 0.1514 |
| $A_3$ | 0.050 | 1813.8 | 48.82 | 0.0269 | 350.8 | 11.93 | 0.1342 |
| $A_4$ | 0.075 | 2078.2 | 49.32 | 0.0237 | 349.6 | 10.48 | 0.1205 |
| $A_5$ | 0.100 | 1991.2 | 36.15 | 0.0182 | 349.8 | 8.019 | 0.0949 |

Quantitative analyses of the two phases were performed using the main diffraction peak area ratios (see Table 1) obtained using the X'Pert HighScore Plus software.[23–26] We use the symbol "$u$" to designate the mass ratio of the $Mn_3O_4$ phase to the perovskite phase. According to XRD theory we then have

$$u = \frac{W_M}{W_P} = \frac{A_M/K_M}{A_P/K_P} = \frac{A_M}{A_P}\frac{K_P}{K_M}, \tag{1}$$

where $W_M$ and $W_P$ denote the masses of the $Mn_3O_4$ phase and the perovskite phase; $A_M$ and $A_P$ are the main diffraction peak areas of the $Mn_3O_4$ phase and perovskite phase; $K_M$ and $K_P$ are the RIR values of the $Mn_3O_4$ phase and the perovskite phase $La_{0.7}Sr_{0.3}MnO_3$. The RIR values are taken from the ICDD (International Centre for Diffraction Data) standard cards 01-080-0382 and 01-089-4461. In other words, they each represent the ratio of the main diffraction peak area of the compound in question to that of $\alpha$-$Al_2O_3$ when the mass ratio is 1:1. Consequently, the values of $K_M$ and $K_P$ are 2.79 and 5.44 respectively. Because the composition and density of the perovskite phase in our samples are different from those of pure $La_{0.7}Sr_{0.3}MnO_3$, the value of $K_P$ used in this expression should be taken as inversely proportional to the density of the samples. Equation (1) can then be rewritten as

$$\begin{aligned} u &= \frac{W_M}{W_P} = \frac{A_M}{A_P}\frac{K_P}{K_M}\frac{d_0}{Zm_P/0.6022V_C} \\ &= 0.6022\frac{A_M}{A_P}\frac{K_P}{K_M}\frac{d_0V_C}{Zm_P}, \end{aligned} \tag{2}$$

where $m_p$ is the molar mass of the perovskite phase, and $V_C$ is the zeroth-order approximation to the cell volume of the perovskite phase, expressed in units of grams (g) and Å$^3$, respectively. $d_0 = 6.447$ is the density of $La_{0.7}Sr_{0.3}MnO_3$. $Z$ gives the number of $ABO_3$ formula units in each cell in the perovskite phase. Because our samples have rhombohedral structure, $Z = 6$. Setting

$$c_M = 0.1004\frac{A_M}{A_P}\frac{K_P}{K_M}d_0V_C, \tag{3}$$

and then, from Eqs. (2) and (3), we have

$$\frac{W_M}{W_P} = \frac{c_M}{m_P}. \tag{4}$$

According to the thermal equilibrium theory of crystal defects,[16,23–26] for the perovskite phase, because the available volume of the $B$ site is smaller than that of the $A$ site, the ions should first occupy the $A$ sites during heat treatment, i.e. if there are vacancies in the perovskite phase, vacancies should be at the $B$ sites. In these self-doped manganites, the sum of the numbers of La and Sr ions is less than that for Mn, and the ratio of the number of lattice points at the $A$, $B$, and O sites in the normal perovskite structure is 1:1:3, resulting in a part of the Mn ions being required to enter into $A$ sites of the perovskite phase in the form of $Mn^{2+}$ ions, while another portion of the Mn ions escaped from the perovskite phase and formed a second $Mn_3O_4$ phase. The reason for this phenomenon may be that the effective radius of $Mn^{2+}$ ion is far smaller than the average effective radius of both $La^{3+}$ and $Sr^{2+}$ ions. In the case of the $A$ sites of the $ABO_3$ structure with coordination number 12, the effective radius of the $Mn^{2+}$ ion is 0.113 nm. $La^{3+}$ and $Sr^{2+}$ ions, on the other hand, have radii of 0.136 nm and 0.144 nm, respectively.[23]

We designate the molar number of Mn cations by $y$ in the $Mn_3O_4$ phase per mole of sample. Then $1-y$ moles of Mn enter into the perovskite phase. We set $M_I$ to be the total number of moles of Mn ions in the perovskite phase per mole of sample with the nominal composition $La_{0.7}Sr_{0.1}Ag_xMnO_{3-\delta}$. Then we have

$$M_I = 1 - y. \tag{5}$$

The molar content of the perovskite phase is then $(0.7+0.1+x+M_I)/2 = (0.8+x+M_I)/2$, and the molar content of the oxygen is $3(0.8+x+M_I)/2$. The masses of the $Mn_3O_4$ and

the perovskite phases per mole of sample are $228.82y/3$ and $(0.8+x+M_{\rm I})m_{\rm p}/2$, respectively. We then have

$$W_{\rm P} = (0.8+x+M_{\rm I})m_{\rm P}/2. \tag{6}$$

Substituting Eq. (6) into Eq. (4), we have

$$\begin{aligned} W_{\rm M} &= (0.8+x+M_{\rm I})c_{\rm M}/2, \\ 76.27y &= (0.8+x+M_{\rm I})c_{\rm M}/2. \end{aligned} \tag{7}$$

Substituting Eq. (5) into Eq. (7), we have

$$y = \frac{(1.8+x)c_{\rm M}}{152.54+c_{\rm M}}. \tag{8}$$

We note that the second ionization energy (21.49 eV) of Ag is close to the third ionization energy of La (19.18 eV). Therefore, we consider that Ag ions in the $A$ sites of the perovskite phase are in the form of $Ag^{2+}$ ions.

For our powder samples sintered at 1073 K, we assume on the basis of the thermal equilibrium theory of crystal defects,[23–26] that there were no vacancies in the $A$ sites of the perovskite phase of the samples and that the missing cations at the $A$ sites were filled by $Mn^{2+}$ ions. Assuming that the perovskite phase in all the samples had the standard $ABO_3$ structure, we can calculate the ion content ratios at the $A$, $B$, and O sites in the perovskite phase. Accordingly, we assume that there are $La^{3+}$, $Sr^{2+}$, $Ag^{2+}$, and $Mn^{2+}$ ions at the $A$ sites of the perovskite phase and that there are $Mn^{3+}$ and $Mn^{4+}$ ions at the $B$ sites.

For notational convenience, we represent the molar amounts of $La^{3+}$, $Sr^{2+}$, $Ag^{2+}$, $Mn^{2+}$, $Mn^{3+}$, $Mn^{4+}$, and $O^{2-}$ in the perovskite phase by $L$, $S$, $A_2$, $M_2$, $M_3$, $M_4$, and $O_2$, respectively. Thus we have

$$M_2 + M_3 + M_4 = M_{\rm I}. \tag{9}$$

Since the molar fraction of the lattice points at the $A$ sites is equal to that of the $B$ sites,

$$L + S + M_2 + A_2 = M_3 + M_4. \tag{10}$$

Furthermore, the number of $O^{2-}$ ions is three times the number of cations at the $A$ sites, giving

$$O_2 = 3(L+S+A_2+M_2). \tag{11}$$

Upon balancing valences

$$3L + 2S + 2A_2 + 2M_2 + 3M_3 + 4M_4 = 2O_2. \tag{12}$$

From Eqs. (9) and (10)

$$M_2 = (M_{\rm I} - A_2 - L - S)/2. \tag{13}$$

Substituting Eq. (13) into Eqs. (10) and (11), we have

$$O_2 = 3(M_{\rm I} + A_2 + L + S)/2, \tag{14}$$

$$M_{\rm I} + L + S + A_2 = 2M_3 + 2M_4. \tag{15}$$

Substituting Eqs. (13) and (14) into Eq. (12)

$$2M_{\rm I} + L + 2S + 2A_2 = 3M_3 + 4M_4. \tag{16}$$

Finally, from Eqs. (15) and (16), we have

$$M_3 = L, \tag{17}$$

$$M_4 = (M_{\rm I} + S + A_2 - L)/2. \tag{18}$$

Therefore, for the perovskite phase and $Mn_3O_4$ phase in our samples, the system can be written as $La^{3+}_{0.7}$ $Sr^{2+}_{0.1}$ $Ag^{2+}_{x}Mn^{2+}_{(0.2-y-x)/2}$ $Mn^{3+}_{0.7}$ $Mn^{4+}_{0.2+0.5x-0.5y}O^{2-}_{1.5(1.8+x-y)}/(Mn_3O_4)_{y/3}$.

The contents of the various ions were calculated using $L = 0.7$ and $S = 0.1$, as shown in Table 2. In Table 2, $R_{\rm M4}$ representing the $Mn^{4+}$ ion content ratio at the $B$ sites of the $ABO_3$ structure, is defined by

$$R_{\rm M4} = \frac{M_4}{M_4 + M_3}. \tag{19}$$

For convenience of interpretation, we also show, in Table 3, the same ion contents normalized so that the $O^{2-}$ content is 3, which is appropriate for the standard $ABO_3$ structure. Consequently, the standard $ABO_3$ structure can be written as $(La_{0.7}Sr_{0.1}Ag_xMn_{1-y})_{2/(1.8+x-y)}O_3$. We can see that, as shown in Table 3, the content of $Mn^{4+}$ ions increases with increasing doping level $x$.

Using directly the contents of the various ions as given in Table 3, the XRD diffraction data were fitted using the Rietveld powder diffraction profile fitting technique. The results are shown in Fig. 2 and Table 4. In Fig. 2, "+" represents the experimental data. Solid lines depict the fitted data. The bottom lines show the difference between the experimental and fitted data.

It may be seen from Table 4 that the final fitting parameters, goodness of fit indicator $s$, profile factor $R_{\rm p}$ and weighted profile factor $R_{\rm wp}$ are satisfactory, indicating that the contents of the various ions calculated by the above method are reasonable.

From Table 4, it may be seen that the lattice parameters $a$ and $c$, the cell volume $V$, the Mn–O bond length, $d$, and the Mn–O–Mn bond angle, $\theta$, do not change in any significant way.

From the fitted results, we can also obtain the percentages of the $Mn_3O_4$ phase ($W_2$ (%)) and the perovskite phase ($W_1$ (%)). Note that the content of the $Mn_3O_4$ phase decreases with increasing doping level $x$ (except for $x = 0.025$).

**Table 2.** The molar contents $L$, $S$, $A_2$, $M_2$, $M_3$, $M_4$, and $O_2$ of $La^{3+}$, $Sr^{2+}$, $Ag^{2+}$, $Mn^{2+}$, $Mn^{3+}$, $Mn^{4+}$, and $O^{2-}$ ions in the perovskite phase per mole of sample, and the $Mn^{4+}$ ion content ratio, $R_{M4}$, at the $B$ sites.

| $x$ | $A$ sites | | | | $B$ sites | | $O_2$ | $R_{M4}$ |
|---|---|---|---|---|---|---|---|---|
| | $L$ | $S$ | $A_2$ | $M_2$ | $M_3$ | $M_4$ | | |
| 0.000 | 0.700 | 0.100 | 0.000 | 0.0194 | 0.700 | 0.1194 | 2.4580 | 0.1457 |
| 0.025 | 0.700 | 0.100 | 0.025 | 0.0118 | 0.700 | 0.1368 | 2.5105 | 0.1635 |
| 0.050 | 0.700 | 0.100 | 0.050 | 0.0079 | 0.700 | 0.1579 | 2.5738 | 0.1841 |
| 0.075 | 0.700 | 0.100 | 0.075 | 0.0022 | 0.700 | 0.1772 | 2.6317 | 0.2020 |
| 0.100 | 0.700 | 0.100 | 0.100 | 0.0026 | 0.700 | 0.2026 | 2.7077 | 0.2245 |

**Table 3.** The molar contents $L$, $S$, $A_2$, $M_2$, $M_3$, $M_4$, and $O_2$ of $La^{3+}$, $Sr^{2+}$, $Ag^{2+}$, $Mn^{2+}$, $Mn^{3+}$, $Mn^{4+}$, and $O^{2-}$ ions, and molar mass $m_P$ of the perovskite phase when the contents of the $O^{2-}$ ions are normalized to 3.

| $x$ | $A$ sites | | | | $B$ sites | | $O_2$ | $m_P$ |
|---|---|---|---|---|---|---|---|---|
| | $L$ | $S$ | $A_2$ | $M_2$ | $M_3$ | $M_4$ | | |
| 0.000 | 0.8543 | 0.1221 | 0.0000 | 0.0236 | 0.8543 | 0.1457 | 3.000 | 232.3 |
| 0.025 | 0.8370 | 0.1200 | 0.0299 | 0.0141 | 0.8365 | 0.1635 | 3.000 | 232.8 |
| 0.050 | 0.8159 | 0.1166 | 0.0583 | 0.0092 | 0.8159 | 0.1841 | 3.000 | 232.8 |
| 0.075 | 0.7980 | 0.1140 | 0.0855 | 0.0025 | 0.7980 | 0.2020 | 3.000 | 233.0 |
| 0.100 | 0.7756 | 0.1108 | 0.1108 | 0.0028 | 0.7756 | 0.2244 | 3.000 | 232.3 |

**Table 4.** Rietveld fitted results of the XRD diffraction patterns for the samples, where $R_p$, $R_{wp}$, and $s$ are the profile factor, weighted profile factor, and goodness of fit indicator, respectively; $a$ and $c$ are the lattice parameters; $V$, $d$, and $\theta$ are the cell volume, Mn–O bond length and the Mn–O–Mn bond angle of the perovskite phase, respectively. The atomic coordinates at $A$, $B$, and O sites are (0, 0, 0.25), (0, 0, 0), and ($x_O$, 0, 0.25), respectively.

| $x$ | $W_1$/% | $W_2$/% | $s$ | $R_p$/% | $R_{wp}$/% | $a$/Å | $c$/Å | $V$/Å$^3$ | $x_o$ | $d$/Å | $\theta$/(°) |
|---|---|---|---|---|---|---|---|---|---|---|---|
| 0.000 | 95.66 | 4.34 | 1.19 | 3.91 | 5.03 | 5.508 | 13.37 | 351.3 | 0.4593 | 1.954 | 166.8 |
| 0.025 | 94.91 | 5.09 | 1.23 | 4.18 | 5.24 | 5.508 | 13.37 | 351.3 | 0.4574 | 1.956 | 166.2 |
| 0.050 | 95.84 | 4.16 | 1.26 | 4.20 | 5.29 | 5.507 | 13.37 | 351.0 | 0.4539 | 1.958 | 165.1 |
| 0.075 | 95.97 | 4.03 | 1.20 | 3.96 | 5.03 | 5.499 | 13.36 | 349.9 | 0.4599 | 1.952 | 167.0 |
| 0.100 | 96.33 | 3.67 | 1.23 | 4.04 | 5.10 | 5.500 | 13.37 | 350.1 | 0.4579 | 1.953 | 166.4 |

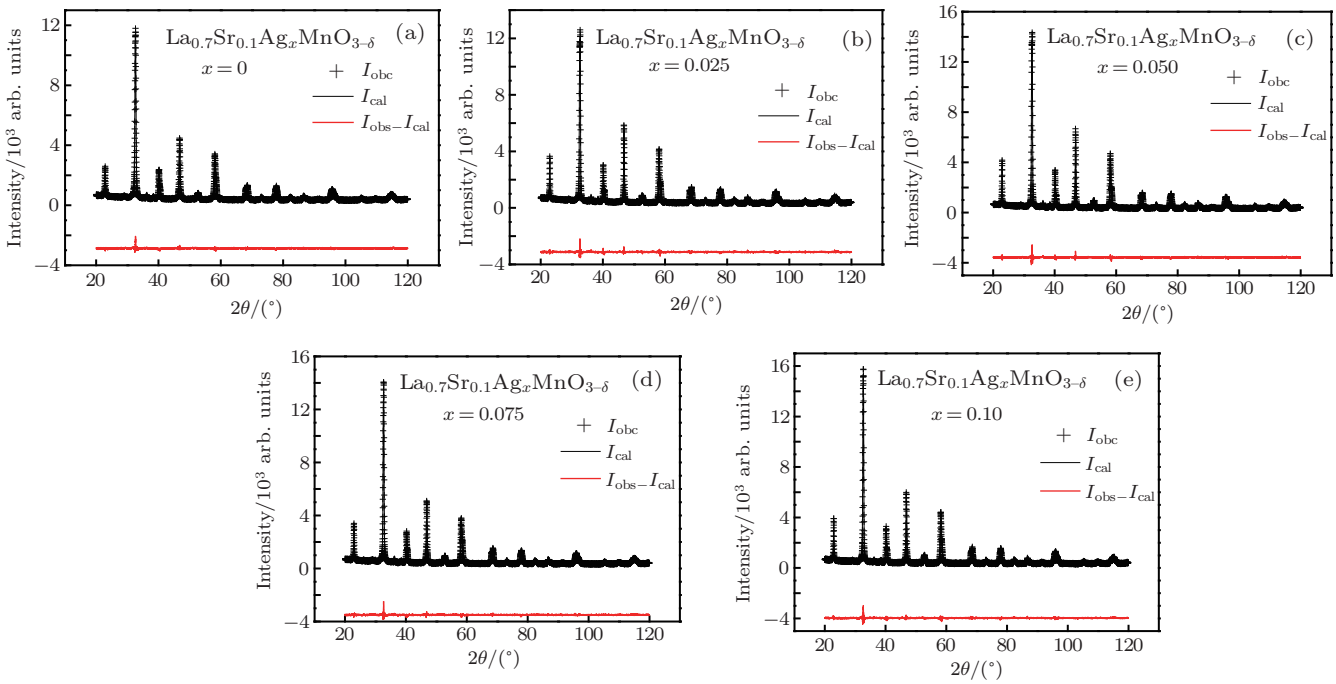



**Fig. 2.** (color online) The Rietveld fitted results for the XRD diffraction patterns of the samples $La_{0.7}Sr_{0.1}Ag_xMnO_{3-\delta}$. Here, "+" and the line represent the experimental and calculated intensities $I_{obs}$ and $I_{cal}$, respectively. The bottom lines show the difference $I_{obs} - I_{cal}$ between the experimental data and the calculated curve.

### 3.2. X-ray energy dispersive spectra (EDS)

X-ray energy-dispersive spectra (EDS) were used to study the elemental content ratios of the $La_{0.7}Sr_{0.1}Ag_xMnO_{3-\delta}$ samples. The element Ag was detected clearly in the EDS patterns, as shown in Fig. 3 and Table 5. Here, $R_O$ and $R_C$ are the atomic concentration ratios of Ag to La, obtained using EDS and calculated using the nominal composition, respectively. Figure 4 shows the dependences of the $R_O$ and $R_C$ on the Ag doping level $x$. It can be seen from Fig. 4 that $R_O$ is very close to $R_C$, which indicates that the Ag ions are doped into the perovskite phase.

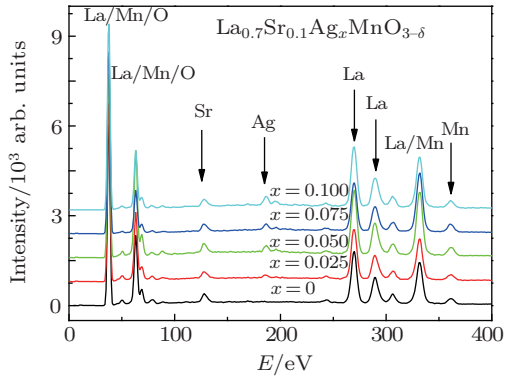



**Fig. 3.** (color online) EDS patterns for the samples with the nominal composition $La_{0.7}Sr_{0.1}Ag_xMnO_{3-\delta}$.

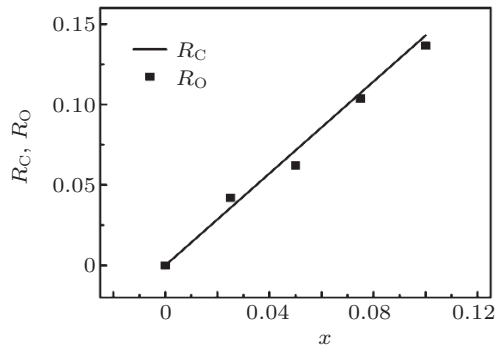



**Fig. 4.** (color online) Curves of the atomic concentration ratio of Ag to La, obtained using EDS (points) and calculated (line) using the nominal composition.

**Table 5.** Contents of various ions in $La_{0.7}Sr_{0.1}Ag_xMnO_{3-\delta}$ measured using EDS. $R_O$ and $R_C$ are the measured and calculated atomic concentration ratios of Ag to La.

| $x$ | O | Mn | Sr | Ag | La | $R_O$ | $R_C$ |
|---|---|---|---|---|---|---|---|
| | atom/% | atom/% | atom/% | atom/% | atom/% | | |
| 0.000 | 66.09 | 17.82 | 1.91 | 0.00 | 14.18 | 0.0000 | 0.0000 |
| 0.025 | 66.16 | 17.81 | 1.49 | 0.59 | 13.96 | 0.0421 | 0.0357 |
| 0.050 | 64.93 | 18.05 | 1.52 | 0.91 | 14.59 | 0.0621 | 0.0714 |
| 0.075 | 67.07 | 16.84 | 1.66 | 1.36 | 13.08 | 0.1036 | 0.1071 |
| 0.100 | 67.03 | 16.51 | 1.73 | 1.77 | 12.96 | 0.1366 | 0.1429 |

### 3.3. Magnetic analysis

Figure 5 shows the curves for the specific magnetization of the samples versus the applied field, measured at 10 K and 300 K. We can see that the coercivity is very small. The specific saturation magnetizations at 10 K show no significant variations. However, the specific saturation magnetizations at 300 K increase from 32.0 A·m$^2$/kg when $x = 0.00$ to 46.8 A·m$^2$/kg when $x = 0.10$. Figure 6(a) shows curves of the specific magnetization, $\sigma$, versus temperature, $T$. Figure 6(b) shows curves of $d\sigma/dT$ versus $T$. According to Fig. 6(b), the absolute value of $d\sigma/dT$ reaches its maximum value when $T = T_C$. We define the temperature $T_C$ as the Curie temperature. It can be seen from Fig. 6(b) that the Curie temperature of samples increases from 310 K when $x = 0.00$ to 328 K when $x = 0.10$, which is the reason why the specific saturation magnetizations at 300 K increase from 32.0 A·m$^2$/kg when $x = 0.00$ to 46.8 A·m$^2$/kg when $x = 0.10$.

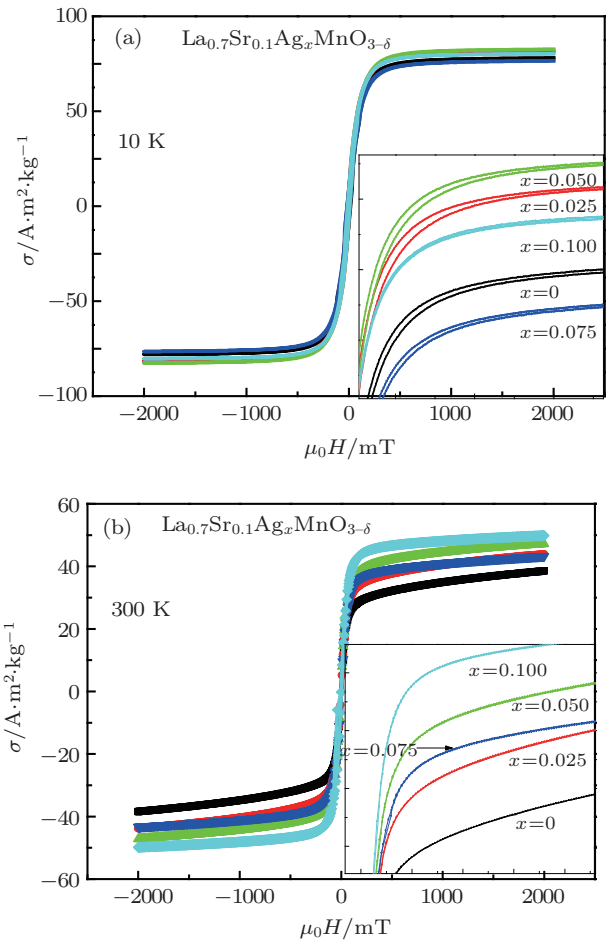



**Fig. 5.** (color online) Curves of the specific magnetization $\sigma$ of the samples of $La_{0.7}Sr_{0.1}Ag_xMnO_{3-\delta}$ versus the applied field, measured at 10 K (a) and 300 K (b).

Combining with Table 3, we can see that the content of $La^{3+}$ ions at the $A$ sites gradually decreases, the total content of $Sr^{2+}$, $Mn^{2+}$, and $Ag^{2+}$ increases, and the content of $Mn^{4+}$ ions at the $B$ sites also gradually increases, with increasing Ag-doping level $x$. Therefore the variation of the Curie temperature of the Ag-doped samples versus the $Mn^{4+}$ ion content is similar to that found in previous studies of $La_{1-x}Sr_xMnO_3$,

which can be explained using the double exchange interaction theory.[1,29]

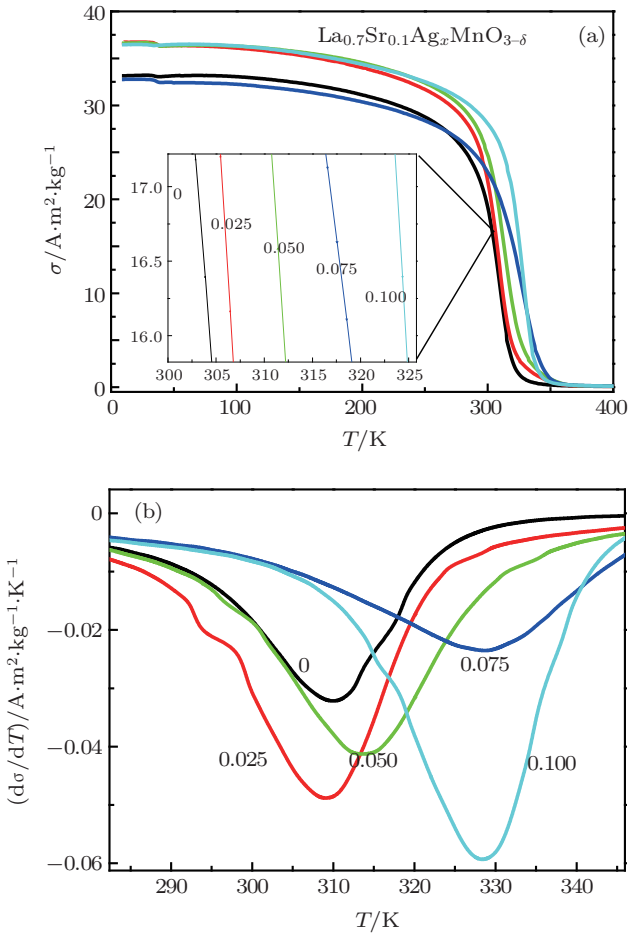



**Fig. 6.** (color online) Curves of the specific magnetization $\sigma$ of the samples $La_{0.7}Sr_{0.1}Ag_xMnO_{3-\delta}$ versus temperature at an applied field of 0.05 T (a) and curves of $d\sigma/dT$ versus temperature (b).

In particular, it should be noted that the atomic concentration ratios of La, Sr, and Mn in our five samples remained essentially the same while the Ag concentration changed. As a result, if there were no Ag cations in the perovskite phase, there should be no significant variation in the magnetic properties. Therefore, the variations of the specific saturation magnetization at 300 K and the Curie temperature suggest that Ag cations have been doped into the *A* sites of perovskite phase in our samples.

## 4. Conclusion

We have successfully prepared perovskite manganite samples with nominal composition $La_{0.7}Sr_{0.1}Ag_xMnO_{3-\delta}$ ($0.00 \leq x \leq 0.10$) using the sol–gel method. In the thermal treatment process, the method of increasing the temperature was improved by increasing the temperature in steps of 50 K, from 473 K to 773 K, with 30 min spent at each step, rather than directly increasing the temperature in one step. X-ray energy dispersive spectra showed that the observed atomic concentration ratios of Ag and La were very close to the nominal atomic concentration ratios. As increasing Ag-doping level $x$, there are the increasing tendencies for both of the specific saturation magnetizations at 300 K and the Curie temperature of the samples. Especially, the specific saturation magnetization of the sample with $x = 0.10$ is distinctly higher than that of the sample with $x = 0.00$ at 300 K, while the Curie temperature of the sample with $x = 0.10$ is distinctly higher than that of the sample with $x = 0.00$.

Because the atomic concentration ratios of La, Sr, and Mn in the five samples were all essentially the same and only the Ag content changed, the variation of the specific saturation magnetizations at 300 K and the Curie temperatures suggest that Ag cations have been doped into the *A* sites of perovskite phase in our samples.

## Acknowledgment

The authors wish to thank Dr. Norm Davison for helpful discussion.

## References

[1] Myron B S and Marcelo J 2001 *Rev. Mod. Phys.* **73** 583
[2] Arafat S S 2014 *Chin. Phys. B* **23** 066101
[3] Cai L G, Liu F M and Zhong W W 2010 *Chin. Phys. B* **19** 097101
[4] Cao X S and Chen C L 2009 *Chin. Phys. B* **18** 2928
[5] Huang W G, Zhang X Q, Li G K, Sun Y, Li Q A and Cheng Z H 2009 *Chin. Phys. B* **18** 5034
[6] Tang G D, Hou D L, Li Z Z, Zhao X, Qi W H, Liu S P and Zhao F W 2006 *Appl. Phys. Lett.* **89** 261919
[7] Tang G D, Liu S P, Zhao X, Zhang Y G, Ji D H, Li Y F, Qi W H, Chen W and Hou D L 2009 *Appl. Phys. Lett.* **95** 121906
[8] Tang G D, Hou D L, Chen W, Zhao X and Qi W H 2007 *Appl. Phys. Lett.* **90** 144101
[9] Zener C 1951 *Phys. Rev.* **82** 403
[10] Brion S D, Ciorcas F, Chouteau G, Lejay P, Radaelli P and Chaillout C 1999 *Phys. Rev. B* **59** 1304
[11] Kim S J, Kim C S, Park S I and Lee B W 2001 *J. Appl. Phys.* **89** 7416
[12] Walha I, Ehrenberg H, Fuess H and Cheikhrouhou A 2009 *J. Alloys Compd.* **485** 64
[13] Dezanneau G, Audier M, Vincent H, Meneghini C and Djurado E 2004 *Phys. Rev. B* **69** 014412
[14] Ramzi H, Narjes H B, Habib B and Christian M 2009 *Solid State Sci.* **11** 885
[15] Sankar C R and Joy P A 2005 *Phys. Rev. B* **72** 024405
[16] Tang G D, Hou D L, Chen W, Hao P, Liu G H, Liu S P, Zhang X L and Xu L Q 2007 *Appl. Phys. Lett.* **91** 152503
[17] Abou-Ras D, Boujelben W, Rouhou A C, Pierre J, Renard J P, Reversat L and Shimizu K 2001 *J. Magn. Magn. Mater.* **233** 147
[18] Ulyanov A N, Yang D S, Chau N, Yu S C and Yoo S I 2008 *J. Appl. Phys.* **103** 07F722
[19] Tao T, Cao Q Q, Gu K M, Xu H Y, Zhang S Y and Du Y W 2000 *Appl. Phys. Lett.* **77** 723
[20] Khare N, Moharil U P, Gupta A K, Singh H K and Srivastava O N 2001 *J. Appl. Phys.* **89** 3532
[21] Li J, Kong C, Zhan Q and Li D X 2002 *J. Phys.: Condens. Matter* **14** 6341
[22] Xu Q Y, Wang R P and Zhang Z 2005 *Phys. Rev. B* **71** 092401
[23] Liu S P, Tang G D, Hao P, Xu L Q, Zhang Y G, Qi W H, Zhao X, Hou D L and Chen W 2009 *J. Appl. Phys.* **105** 013905
[24] Liu S P, Xie Y, Xie J and Tang G D 2011 *J. Appl. Phys.* **110** 123714
[25] Liu S P, Xie Y, Tang G D, Li Z Z, Ji D H, Li Y F and Hou D L 2012 *J. Magn. Magn. Mater.* **324** 1992
[26] Liu S P, Liu S P, Li Z Z, Ji D H, Li Y F, Chen W and Hou D L 2011 *Physica B* **406** 869
[27] Chen W, Zhong W, Hou D L, Gao R W, Feng W C, Zhu M G and Du Y W 2002 *J. Phys.: Condens. Matter* **14** 11889
[28] Ji D H, Tang G D, Li Z Z, Han Q J, Hou X, Bian R R and Liu S R 2012 *J. Appl. Phys.* **111** 113902
[29] Urushibara A, Moritomo Y, Aima T, Asamitsu A, Kido G and Tokura Y 1995 *Phys. Rev. B* **51** 14103